Draft version November 19, 2024
Typeset using LaTeX default style in AASTeX631

The Ubiquity of Twisted Flux Ropes in the Quiet Sun*

Tahar Amari,[1] Aurélien Canou,[1] Marco Velli,[2] Zoran Mikic,[3] Frederic Alauzet,[4] Eric Buchlin,[5] Jean-François Luciani,[1] Jean -Jacques Aly,[6] and Lucas A. Tarr[7]

[1] *CNRS, Centre de Physique Théorique de l'Ecole Polytechnique, IPP, F-91128 Palaiseau Cedex, FRANCE*
[2] *Department of Earth, Planetary Space Sciences University of California, Los Angeles, CA 90095-1567.USA.*
[3] *Predictive Science Inc. 9990 Mesa Rim Rd, Suite 170 San Diego, CA 92121. USA.*
[4] *INRIA Saclay Ile-de-France, Projet Gamma3, 1, rue Honoré d'Estienne d'Orves, 91126 Palaiseau, France*
[5] *Université Paris-Saclay, CNRS, Institut d'Astrophysique Spatiale Orsay France*
[6] *AIM - Unité Mixte de Recherche CEA - CNRS Université Paris VII - UMR no 7158, Centre d'Etudes de Saclay, F-91191 Gif sur Yvette Cedex, FRANCE*
[7] *National Solar Observatory.22 Ohia Ku St Makawao, HI 96768.USA.*

ABSTRACT

Models and observations have demonstrated that Twisted Flux Ropes (TFRs) play a significant role in the structure and eruptive dynamics of active regions. Their role in the dynamics of the quiet Sun atmosphere on has remained elusive, their fundamental relevance emerging mainly from theoretical models (Amari et al. 2015), showing that they form and erupt as a result of flux cancellation. Here HINODE high-resolution photospheric vector magnetic field measurements are integrated with advanced environment reconstruction models: TFRs develop on various scales and are associated with the appearance of mesospots. The developing TFRs contain sufficient free magnetic energy to match the requirements of the recently observed "campfires" discovered by Solar Orbiter in the quiet Sun. The free magnetic energy is found to be large enough to trigger eruptions while the magnetic twist large enough to trigger confined eruptions, heating the atmosphere. TFRs are also connected to larger scale magnetic fields such as supergranulation loops, allowing the generation of Alfvén waves at the top of the chromosphere that can propagate along them. High-resolution magnetohydrodynamic simulations, incorporating subsurface dynamo activity at an unprecedented 30 km spatial resolution, confirm that TFRs are ubiquitous products of the permanent small scale dynamo engine that feeds their formation, destabilization, eruption via flux emergence, submergence and cancellation of their chromospheric feet, similar to the dynamics driving large scale eruptive events. Future investigations, especially with the Daniel K. Inouye Solar Telescope (DKIST) and Solar Orbiter will deepen our understanding of TFRs in the context of atmospheric heating.

Keywords: magnetohydrodynamics (MHD) — stars: coronae — stars: magnetic field — stars: flare — Sun: coronal mass ejections (CMEs) — Sun: flares

1. INTRODUCTION

The quiet Sun, defined as a region of the outer solar atmosphere not dominated by the strong magnetic activity of sunspots and active regions, constitutes the largest portion of the solar surface, persisting throughout the solar cycle. However, since the observations from SOHO it has been shown that the quiet Sun is also incredibly dynamic, exhibiting a wide range of bursty structures, from the spicules well known from H-alpha observations to mottles, blinkers, jets, tornadoes, and the recently observed Solar Orbiter EUV brightenings nicknamed "campfires" (Berghmans et al. 2021),

* Released on March, 1st, 2021

extending to various heights from the chromosphere to the core corona. Understanding how these phenomena are related to underlaying structures and their contribution to the heating of the solar atmosphere – and reconciling the heating with observations at various altitudes – remain major challenges (Aschwanden et al. 2007).

Although it is not known whether the physical mechanisms responsible for the thermal structuring of the Quiet Sun's atmosphere begin immediately above the temperature minimum, they are certainly active at an altitude of 4000 km. While this zone remotely observed by the Solar Orbiter, is found very active, it remains out of reach of in-situ measurements for the foreseeable future. Characterizing the underlying magnetic structures associated with heating mechanisms, such as their length scales, is thus of paramount importance.

A fundamental discovery on the nature of the quiet Sun was the observation that small-scale magnetic fields (Lites et al. 2008; Trujillo Bueno et al. 2004), and particularly horizontal ones, dominate its structure. It is thus important to investigate how such small scale internetwork magnetic fields are related to the larger supergranular network magnetic fields emerging above (Gošić et al. 2024).

Over the past decades, Twisted Flux Ropes (TFRs) have been recognized as crucial structures for understanding the magnetic structure and support of prominences (Kuperus & Raadu 1974; Anzer & Priest 1985; Amari & Aly 1989; Démoulin & Priest 1988; van Ballegooijen & Martens 1989; Aulanier & Démoulin 1998) and the mechanisms behind solar eruptions (Aly & Amari 1985; Low 2001; Priest & Forbes 2002; Amari & Aly 2009; Török & Kliem 2005; Amari et al. 2014; Aulanier 2014; Amari et al. 2018; Kliem & Török 2006; Török et al. 2018). The formation and evolution of a TFR towards eruption can occur and be modeled in different ways, including the emergence of a pre-existing TFR from the convection zone (Fan 2022). Numerous remarkable studies driven by numerical simulations have been performed, considering different physical ingredients, either idealistically by coupling different zones of the atmosphere (Amari et al. 2004, 2005; Fan & Gibson 2004, 2007) or with more realistic models including the different layers (Archontis & Török 2008; Cheung et al. 2019; Leake et al. 2022). Despite the difficulties in observing convection zone magnetic fields, there is indirect evidence supporting the emergence of such formed TFR (López Fuentes et al. 2000; MacTaggart et al. 2021).

On the other hand, reconstruction of the coronal magnetic field from vector magnetograms above active regions shows the existence and formation of sheared magnetic arcades and TFRs prior to eruption, with the former being a prerequisite stage during the slow evolution leading to TFR and eruption (Patsourakos et al. 2020). Whether the TFR is fully formed before or during the eruption remains a matter of debate. All these studies (theoretical and observational) of active regions have shown that the photospheric transverse magnetic field is a key ingredient for the energization of highly sheared magnetic field structures and TFRs.

The importance of TFRs for the structure and dynamics of the quiet Sun has only been appreciated more recently, as initially suggested by the somewhat idealized numerical simulations of (Amari et al. 2015). It was shown that reconnection provides chromospheric heating as recently found also in active regions (Bose et al. 2024), while in upper layers waves also play a role. The simulations demonstrate that TFRs evolve in response to magnetic flux changes occurring at their chromospheric feet, which eventually leads to their eruption into upper layers, as in some models of coronal mass ejections. Recently more realistic simulations (Chen et al. 2021; Martínez-Sykora et al. 2019; Robinson et al. 2023) have also shown that TFRs may form.

Given the importance of TFRs, it is crucial to examine data in the quiet Sun. While SDO/HMI vector magnetograms have been intensively used in the case of active regions, in Section 2 the present paper makes use of the vector magnetic field data from Hinode, which enables higher spatial resolution and lower noise in particular for the transverse component (Lites et al. 2008; Régnier et al. 2008). The focus is on small-scale vector magnetic field measurements of the quiet Sun by Hinode (Lites et al. 2008). The usual assumption of current-free (potential) magnetic field configuration (Schrijver & Title 2003) is relaxed in Section 3 to allow for force-free magnetic fields using the XTRAPOL model (Amari & Aly 2010) to compute the magnetic structures emerging from the photospheric field measurement. These yield ubiquitous small-scale TFRs in the quiet Sun region. In addition results from a new high resolution (at 30 km) MHD numerical simulation of a small portion of the quiet Sun are also shown that support the reconstruction findings: TFRs, produced by the sub-photospheric dynamo with emergence and cancellation, clearly populate the whole quiet Sun, reaching into the chromosphere and above (Gošić et al. 2024).

2. OBSERVATIONS AND RECONSTRUCTION OF THE MAGNETIC ENVIRONMENT OF A TYPICAL QUIET SUN REGION

To address this problem a region of the quiet Sun located near the disk center on 2007/03/10 (Lites et al. 2008) was targeted. The Spectro-Polarimeter (SP) of the Solar Optical Telescope (SOT, Tsuneta et al. 2008) on board the satellite Hinode (Kosugi et al. 2007) measured the Stokes parameters in normal mode providing a high resolution map with pixel size of (0.148570 ; 0.159992) arcsecs in the (x,y) helioprojective Cartesian coordinates. The level-2 Hinode/SOT/SP data[1] contain the continuum field, the norm of $\mathbf{B}$, the inclination and azimuth angles; the azimuthal angle being known to suffer from the 180°-amibiguity. The azimuthal ambiguity is resolved with the Minimum Energy Method (Leka et al. 2009) applied a thousand times with different seeds to determine statistically the most probable solution. These data are then converted to Cartesian magnetic field components and remapped to a cartesian grid (Gary & Hagyard 1990) with pixel sizes $(dx; dy)$ of $(0.1; 0.1)$ Mm covering an area of $216 \times 114\,\mathrm{Mm}^2$. The current density $J_z\,\hat{\mathbf{z}} = \nabla\times \mathbf{B}_T$ and $\alpha = J_z/B_z$ are computed on that grid as long as $\|B_T\| > 10\,\mathrm{G}$ and $|B_z| > 5\,\mathrm{G}$, respectively. An additional 5-point gaussian smoothing is applied to get rid of abrupt variations. Figure 1 presents the result of this preparation.

It is worth noticing that the region of interest is associated with a period of the declining phase of solar cycle 23, during which no active region was present.

The first few thousand kilometers above the photosphere are extremely dynamic, but as the plasma β decreases quickly with height fundamental insights can be obtained by assuming the atmospheric domain to be filled with a low-β slightly resistive and viscous plasma. Then $\mathbf{B}$ obeys the standard force-free equations (Amari et al. 2014) and can be reconstructed from the observed photospheric field with appropriate boundary conditions at the top and the sides of the domain. The force-free field is obtained using the numerical model XTRAPOL (Amari & Aly 2010) that integrates the equilibrium equations up to an altitude of 80 Mm on a non uniformly distributed grid with a total of 321 points in the vertical direction. Thereafter and without loss of generality we focus on a sub volume of $96\times 70\times 80\,\mathrm{Mm}^3$ that embraces granulation and supergranulation. The horizontal spatial resolution is uniform with $dx = dy = 100\,\mathrm{km}$, while vertically constant $dz = 50\,\mathrm{km}$ up to 8 Mm, and then increasing to reach 750 km at 80 Mm.

The magnetic configuration differs substantially from that of the potential field that has the smallest magnetic energy compatible with the flux distribution at the lower photospheric boundary (Schrijver & Title 2003). One observes field lines that meander and tangle into a number of TFRs, shown in Figure 2. The characteristic TFR length is associated with an intermediate coherent scale we have previous dubbed mesospots (Bushby & Favier 2014; Amari et al. 2015, see section below for the simulation). The presence of a current density $\mathbf{j}$ in the whole volume means that the magnetic field energy in the extrapolted field is much greater than the energy of the associated current-free (potential) magnetic field having the same normal componentat the photosphere).

The TFRs recovered from XTRAPOL have typical apex heights around or below 7 Mm, similar to the heights of the so-called "campfires" (Zhukov et al. 2021) recently observed by Solar Orbiter. To better analyze the magnetic field configuration and its potential for energetic dynamics, a simplified segmentation of the domain was performed, using boxes to encompass single TFRs when possible or several TFRs where the field configuration included close or interlaced twisted fields. In this way more localized estimates of the distribution of the magnetic energy inside the reconstructed domain, and specifically associated with interesting TFRs (Figure 3) were obtained. The values recovered match those estimated by Panesar et al. (2021) to sustain the losses from "campfires" ($10^{26} - 10^{27}$ erg), which require an average magnetic field of the order of 20 G. As shown in Figure 3, the values found in the boxes are of same order and even larger since $9.6\ 10^{26}\,\mathrm{erg} \leq W \leq 6.1\ 10^{28}\,\mathrm{erg}$, while the difference between the magnetic energy and the current-free one is in the interval $7.5\ 10^{25}\,\mathrm{erg} \leq \Delta W \leq 1.2\ 10^{27}$ erg. Furthermore we find that the magnetic energy contained in each box, is larger than that required to trigger non confined eruptions, when compared to the energy of the semi-open field (see Amari et al. 2014). The magnetic twist in individual TFRs is also found to be large, with many values above $\|Tw\| = 2$, favourable to trigger confined eruptions via the kink instability (Amari et al. 2018, and references therein; see bottom panel of Figure 3).

The magnetic topology is highly complex, splitting the domain into many magnetic cells delimited by singular surfaces, the so-called separatrices. This is achieved by computing the so called squashing factor Q (Titov 2007), exhibiting various delimited regions, both in the sense of exact separatrices surfaces (Parker 1983), due to the highly multipolar distribution of magnetic field, and also of Quasi Separatrix Layers (QSLs; Demoulin et al. 1996), where Q is very large. These QSLs contain separated bundles of field lines, becoming zones of observed emission, during the

[1] The L2-data are available at https://csac.hao.ucar.edu/sp_data.php. They have already been inverted from Stokes parameters using the Merlin algorithm (Skumanich & Lites 1987).

evolution of the system as a result of magnetic reconnection. A synthetic emissivity is computed for the extrapolated volume using a method introduced for models of this type which do not evolve the complete plasma dynamics, including thermodynamic quantities such as density and temperatures that are necessary for atomic physics emissivity calculations (Cheung & DeRosa 2012; Amari et al. 2018) such as can be obtained using the CHIANTI package (Dere et al. 1997; Del Zanna et al. 2021). The method is based on a preliminary calculation of millions of field lines, along which the electric current density is then integrated. An emissivity proxy is then defined for each cell of the atmosphere by summing the contributions of each line that passes through that cell. The emissivity of the reconstructed environment is shown in Figure 3-c. Hot spots associated with the large electric currents flowing along lines are clearly visible and bear a striking resemblance to "campfires".

The examined TFRs share several typical properties of their active region counterparts, and may therefore be associated with eruptions in the neighbourhood of mesospots, triggered by mechanisms (such as flux cancellation) similar to those at work in large scale eruptive events (see Amari et al. 2015, and the section below about numerical simulations).

Such TFRs are also coupled to the large scale magnetic fields including super-granulation loops. As shown in Figure 2, the TFR on the bottom right side is located within a dome-shaped structure that opens to large scales, resembling the classical configuration involved in jets. An eruption of this TFR (caused by its large twist/energy) would affect the corona directly through spicule type activity and waves and jets, as already seen in the numerical calculation of Amari et al. (2015) but also characteristic of many observations of eruptive active region magnetic configurations (Schmieder 2022). Owing to those connections with larger scale magnetic field, the perturbations resulting from their possible eruption and reconnection, happening near the top of the chromosphere, generate Alfvén waves that can propagate along the vertical tubes and contribute to heating higher up, which is not considered here. It is worth noting that unlike the typical configurations in Amari et al. (2015), the large scale supergranulation scale loops carry only a small amount of twist in the present force free reconstruction. This is coherent with the fact that equilibrium solutions cannot catch waves. As can be seen in the red rectangle representing the typical size of the MHD simulation $15 \times 15\,\mathrm{Mm}^2$) in Figure 4, the scale of the TFRs which occupies a significant part of the box and which we had described as mesoscale, can be either smaller or larger than this box, but always above the granular scale.

3. NUMERICAL SIMULATION OF THE EMERGENT MAGNETIC FIELD STRUCTURE OF A QUIET SUN REGION

Here we illustrate the formation of dynamic TFRs in the Quiet Sun via numerical simulation. To do so, we build upon the established result that the key source of energy is the small-scale magnetic field, as mentioned earlier in the introduction (Lites et al. 2008; Trujillo Bueno et al. 2004). Our approach is motivated by the aim to explore of understanding the necessary conditions that result from maintaining a hot atmosphere with a sharp transition region, statistically steady constant in time, and of determining the resulting structures that are formed and compatible with the atmosphere. Full details of the method, initially introduced in Amari et al. (2008) and further improved, are provided in Amari et al. (2015), including a comparison of the simulated dynamo-generated surface magnetic field with the fields distribution inferred from observations of scattering polarization in atomic and molecular lines. We briefly recall here the main points of the approach and improvements made.

The magnetic field is assumed to be created by a subsurface small-scale dynamo operating in the upper 1.5 Mm of the convection zone, where the plasma is taken to obey the incompressible Boussinesq MHD equations. This layer is coupled with an atmospheric region described by a different MHD model that includes a photosphere and a chromosphere with respective thicknesses of 0.5 Mm and 1.5 Mm, as in the Sun though the observed extent of the chromosphere fluctuates and may be up to 5 Mm high e.g. in coronal holes, and a corona extending up to 30 Mm. We start from an equilibrium atmosphere solution of the hydrostatic equation with a density profile differing slightly from VAL data. Coupling between the underlying dynamo and the atmosphere is achieved through the Resistive Layer Model (Amari et al. 2015). The atmosphere is initially taken to be in equilibrium, and its temperature is kept constant in time, in line with our aim of maintaining the sharp variations and the saturated dynamo.

A few differences with respect to Amari et al. (2015) are worth noting. The code has been improved with MPI parallelisation, allowing a larger spatial resolution of $512 \times 512 \times 400$ for the same horizontal domain, but now extending vertically to 30 Mm. The fully implicit numerical scheme provides better resolution for the resistive part, and a higher-order scheme for our numerical MHD code METEOSOL has been implemented since its last version (Amari et al.

2015). The mesh is horizontally uniform and vertically uniform in the convection zone, while non-uniform in the atmosphere, with a typical spatial resolution of 0.03 Mm.

After reaching a saturated dynamo, as in the lower resolution simulation, we observed the emergence and submergence of structures. The temperature is structured at the granulation scale while the magnetic field exhibits both granulation scale and mesoscale features, clearly showing that flux cancellation of magnetic concentrations of opposite polarities occurs frequently throughout the evolution. Although on the photosphere the magnetic field appears to be organized at the granulation scale of fluid motions, it also exhibits more persistent (30 minutes lifetime) mesoscale magnetic flux concentrations that play an important role in the system evolution, which we previously called "mesospots" by analogy with active region sunspots with sizes several times that of a granulation cell.

Higher up, as already discovered in Amari et al. (2015), coherent structures that are no longer confined generate emerging motions by expanding into the region above. These structures are present at 1.5 Mm above the surface, where they appear as coherent magnetic flux tubes with a width of about 1–2 Mm and a mean intensity of about 20 G. Among these structures, TFRs appear (Figure 4), with a physics dominated by the relatively stable mesospots. At the periphery of these mesospots, dynamic current sheets persistently structure the plasma and are associated with magnetic complexity. TFRs associated with these mesospots form, and eruptions in the neighbourhood of the mesospots are triggered by mechanisms such as magnetic flux cancellation, similar to those at work in large-scale eruptive events, but occurring at higher altitudes and involving their chromospheric feet. As seen in Figure 4, the horizontal size of the domain corresponds to the smallest rectangle drawn in green in Figure 1, exhibiting several TFRs, which supports the widespread presence of these structures across the entire quiet Sun. While optical decoupling first occurs at the photosphere, beyond which photons freely escape, magnetic decoupling occurs above the Transition Region, with TFRs being a natural consequence. Ongoing and future investigations, especially with the Daniel K. Inouye Solar Telescope (DKIST) and Solar Orbiter, are anticipated to deepen our understanding of those TFRs in the context of atmospheric heating.

Finally, we would like to point out that although one limitation of the reconstruction made using XTRAPOL in Section is that it assumes a force-free hypothesis, which does not include the chromosphere and transition region as in the more realistic coupled MHD simulation model discussed in this section, the fact that these TFRs are also obtained in the coupled MHD simulation provides further evidence for the presence of TFRs. Furthermore, as the TFRs found lower down in the atmosphere might be more confined, the values of twist and energy relative to those of the semi open fields (that provide lower limits for eruption potential) for these TFRs might be even greater than those usually found in pure force-free models. A more in-depth analysis of this simulation, including multiple other aspects beyond the TFRs presented here, will be presented in a forthcoming paper.

This work was granted access to the HPC resources of CINES/IDRIS under the allocation 2021-A0100500438 made by GENCI. The numerical simulations described in this paper have been performed on the HPE SGI 8600, Jean-Zay of the institute I.D.R.I.S of the Centre National de la Recherche Scientifique, through GENCI. We acknowledge support of the Centre National dÉtudes Spatiales (CNES). Ambiguity resolution and 3D diagnostics computations have been performed under the project n3s on the HPC facility Cholesky operated by the Ecole Polytechnique / IDCS. Hinode is a Japanese mission developed and launched by ISAS/JAXA, with NAOJ as domestic partner and NASA and STFC (UK) as international partners. It is operated by these agencies in cooperation with ESA and NSC (Norway).

REFERENCES

Aly, J. J., & Amari, T. 1985, in Theoretical Problems in High Resolution Solar Physics, Vol. 212, MPA, Munchen, 319

Amari, T., & Aly, J. 2009, in IAU Symposium, Vol. 257, IAU Symposium, ed. N. Gopalswamy & D. F. Webb, 211–222, doi: 10.1017/S1743921309029329

Amari, T., & Aly, J. J. 1989, A&A, 208, 261

—. 2010, A&A, 522, A52, doi: 10.1051/0004-6361/200913058

Amari, T., Canou, A., & Aly, J.-J. 2014, Nature, 514, 465, doi: 10.1038/nature13815

Amari, T., Canou, A., Aly, J.-J., Delyon, F., & Alauzet, F. 2018, Nature, 554, 211, doi: 10.1038/nature24671

Amari, T., Luciani, J. F., & Aly, J. J. 2004, ApJL, 615, L165

—. 2005, ApJL, 629, L37

—. 2008, ApJL, 681, L45, doi: 10.1086/590323

Amari, T., Luciani, J.-F., & Aly, J.-J. 2015, Nature, 522, 188, doi: 10.1038/nature14478

Anzer, U., & Priest, E. 1985, SoPh, 95, 263

Archontis, V., & Török, T. 2008, A&A, 492, L35, doi: 10.1051/0004-6361:200811131

Aschwanden, M. J., Winebarger, A., Tsiklauri, D., & Peter, H. 2007, ApJ, 659, 1673, doi: 10.1086/513070

Aulanier, G. 2014, in Nature of Prominences and their Role in Space Weather, ed. B. Schmieder, J.-M. Malherbe, & S. T. Wu, Vol. 300, 184–196, doi: 10.1017/S1743921313010958

Aulanier, G., & Démoulin, P. 1998, A&A, 329, 1125

Berghmans, D., Auchère, F., Long, D. M., & et al. 2021, Astronomy & Astrophysics, 656, A79, doi: 10.1051/0004-6361/202140380

Bose, S., De Pontieu, B., Hansteen, V., et al. 2024, Nature Astronomy, doi: 10.1038/s41550-024-02241-8

Bushby, P. J. & Favier, B. 2014, A&A, 562, A72. doi:10.1051/0004-6361/201322993

Chen, Y., Przybylski, D., Peter, H., et al. 2021, A&A, 656, L7, doi: 10.1051/0004-6361/202140638

Cheung, M. C. M., & DeRosa, M. L. 2012, ApJ, 757, 147, doi: 10.1088/0004-637X/757/2/147

Cheung, M. C. M., Rempel, M., Chintzoglou, G., et al. 2019, Nature Astronomy, 3, 160, doi: 10.1038/s41550-018-0629-3

Del Zanna, G., Dere, K. P., Young, P. R., et al. 2021, ApJ, 909, 38. doi:10.3847/1538-4357/abd8ce

Démoulin, P., & Priest, E. R. 1988, A&A, 206, 336

Demoulin, P., Henoux, J. C., Priest, E. R., et al. 1996, A&A, 308, 643

Dere, K. P., Landi, E., Mason, H. E., et al. 1997, A&AS, 125, 149. doi:10.1051/aas:1997368

Fan, Y. 2022, ApJ, 941, 61, doi: 10.3847/1538-4357/aca0ec

Fan, Y., & Gibson, S. 2007, ApJ, 668, 1232, doi: 10.1086/521335

Fan, Y., & Gibson, S. E. 2004, ApJ, 609, 1123

Gary, G. A., & Hagyard, M. J. 1990, SoPh, 126, 21, doi: 10.1007/BF00158295

Gošić, M., De Pontieu, B., & Sainz Dalda, A. 2024, ApJ, 964, 175, doi: 10.3847/1538-4357/ad2e03

Kliem, B., & Török, T. 2006, Physical Review Letters, 96, 255002, doi: 10.1103/PhysRevLett.96.255002

Kosugi, T., Matsuzaki, K., Sakao, T., et al. 2007, Solar Physics, 243, 3, doi: 10.1007/s11207-007-9014-6

Kuperus, M., & Raadu, M. A. 1974, A&A, 31, 189

Leake, J. E., Linton, M. G., & Antiochos, S. K. 2022, ApJ, 934, 10, doi: 10.3847/1538-4357/ac74b7

Leka, K. D., Barnes, G., Crouch, A. D., et al. 2009, SoPh, 260, 83, doi: 10.1007/s11207-009-9440-8

Lites, B. W., Kubo, M., Socas-Navarro, H., et al. 2008, ApJ, 672, 1237, doi: 10.1086/522922

López Fuentes, M. C., Démoulin, P., Mandrini, C. H., & van Driel-Gesztelyi, L. 2000, ApJ, 544, 540, doi: 10.1086/317180

Low, B. C. 2001, J. Geophys. Res., 106, 25141, doi: 10.1029/2000JA004015

MacTaggart, D., Prior, C., Raphaldini, B., Romano, P., & Guglielmino, S. L. 2021, Nature Communications, 12, 6621, doi: 10.1038/s41467-021-26981-7

Martínez-Sykora, J., De Pontieu, B., Hansteen, V. H., et al. 2019, ApJ, 878, 40, doi: 10.3847/1538-4357/ab1f0b

Panesar, N. K., Tiwari, S. K., Berghmans, D., et al. 2021, ApJL, 921, L20, doi: 10.3847/2041-8213/ac3007

Parker, E. N. 1983, ApJ, 264, 635. doi:10.1086/160636

Patsourakos, S., Vourlidas, A., Török, T., Kliem, B., & Antiochos, S. K. 2020, Space Science Reviews, 216

Priest, E. R., & Forbes , T. G. 2002, Astron Astrophys Rev, 10, 313

Régnier, S., Parnell, C. E., & Haynes, A. L. 2008, A&A, 484, L47, doi: 10.1051/0004-6361:200809826

Robinson, R., Aulanier, G., & Carlsson, M. 2023, Astronomy & Astrophysics, 673, A79, doi: 10.1051/0004-6361/202346065

Schmieder, B. 2022, Frontiers in Astronomy and Space Sciences, 9, 820183, doi: 10.3389/fspas.2022.820183

Schrijver, C. J., & Title, A. M. 2003, ApJL, 597, L165, doi: 10.1086/379870

Skumanich, A., & Lites, B. W. 1987, ApJ, 322, 473, doi: 10.1086/165743

Titov, V. S. 2007, ApJ, 660, 863, doi: 10.1086/512671

Török, T., & Kliem, B. 2005, ApJL, 630, L97, doi: 10.1086/462412

Török, T., Downs, C., Linker, J. A., et al. 2018, ApJ, 856, 75, doi: 10.3847/1538-4357/aab36d

Trujillo Bueno, J., Shchukina, N., & Asensio Ramos, A. 2004, Nature, 430, 326, doi: 10.1038/nature02669

Tsuneta, S., Ichimoto, K., Katsukawa, Y., et al. 2008, Solar Physics, 249, 167, doi: 10.1007/s11207-008-9174-z

van Ballegooijen, A. A., & Martens, P. C. H. 1989, ApJ, 343, 971, doi: 10.1086/167766

Zhukov, Mierla, M., Auchere, F., et al. 2021, A&A, 656, A35, doi: 10.1051/0004-6361/202141010

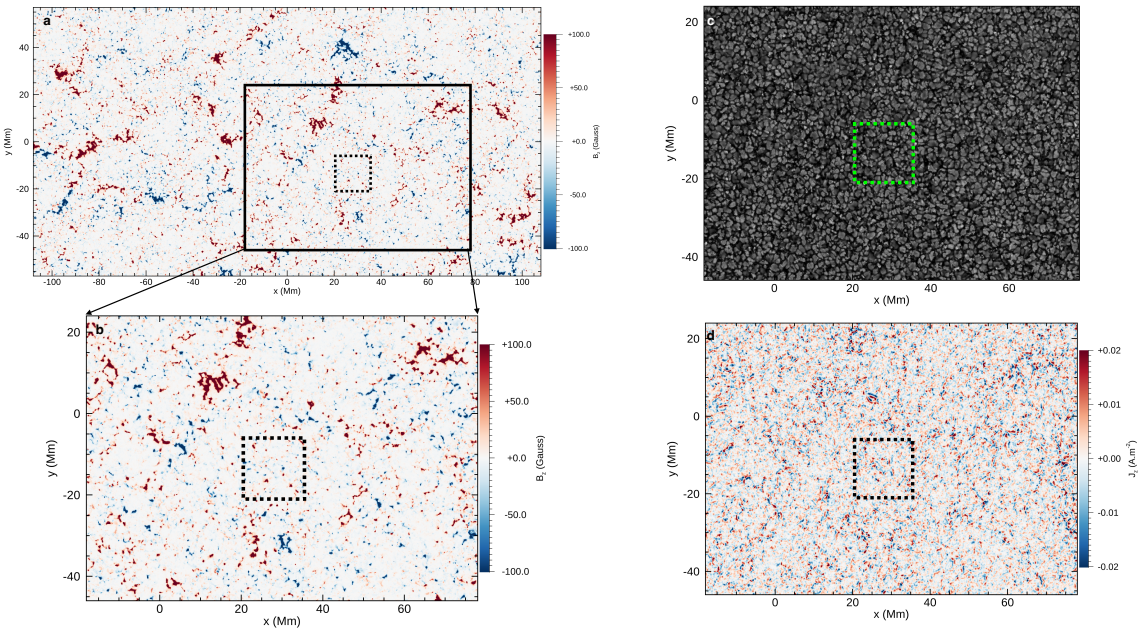

Figure 1. HINODE/SOT high resolution photospheric magnetic map used to build up adapted resolution boundary conditions. a. The normal component B_z of the magnetic field for the full-size magnetogram ($216 \times 114\,\mathrm{Mm}^2$),from which we extract a subdomain (solid line rectangle) of $96 \times 70\,\mathrm{Mm}^2$ corresponding to the domain above which coronal magnetic field is reconstructed of, and within which a smaller one (dashed line) corresponds to the domain of simulation ($15 \times 15\,\mathrm{Mm}^2$). b. Zoom on the normal component B_z for the reconstruction domain. c. Continuum image for the reconstruction domain exhibiting the granulation scale. d. The normal component J_z of the electric current for the reconstruction domain.

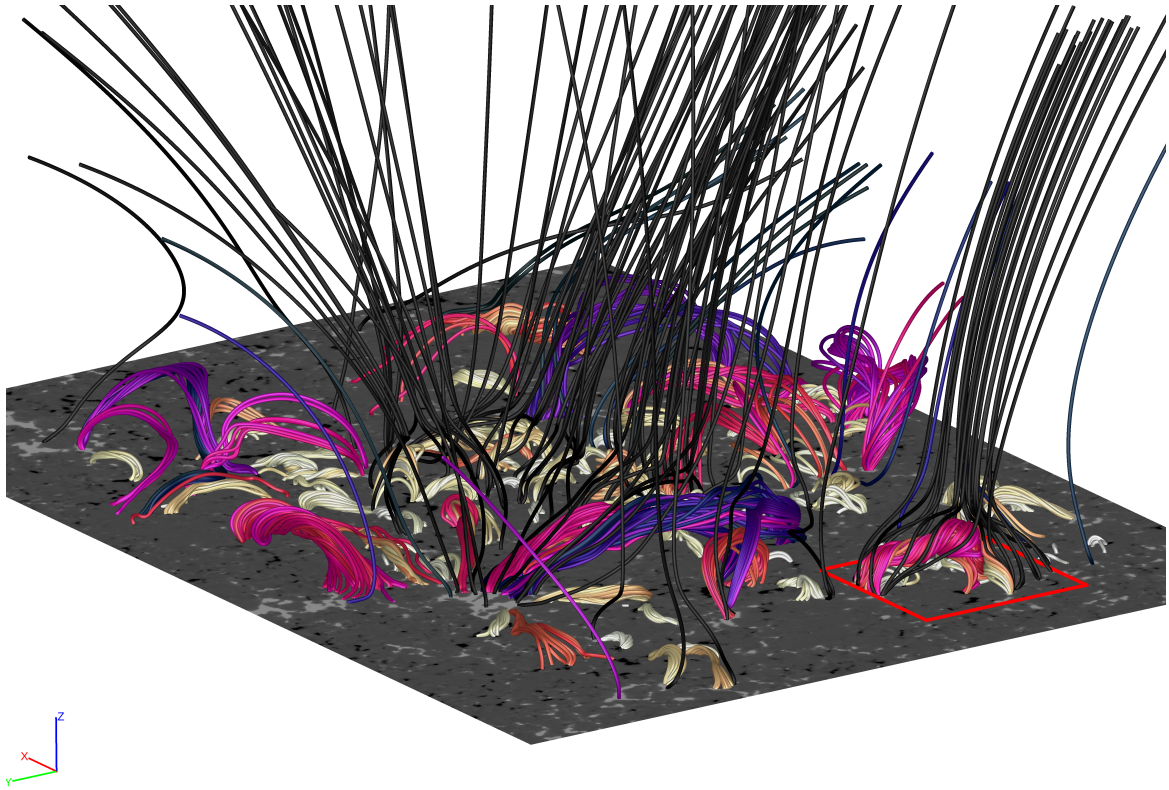

Figure 2. Selected field lines of the magnetic environment above the photosphere using the force-free model XTRAPOL. Twisted Flux Ropes stand around mesospots, both below and above the transition regions. The red rectangle shown on the right, features the same box size as the one of the simulation box in Figure 4.

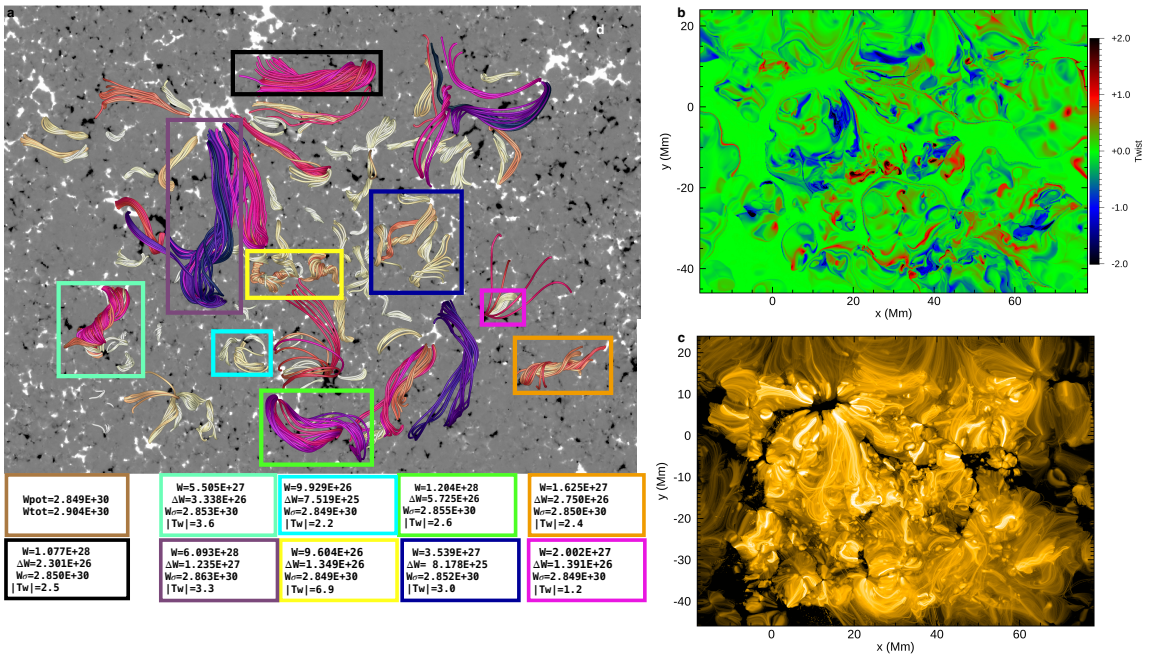

Figure 3. a. Boxes enclosing TFRs used to compute some of their characteristics. Each box can contain one or a few TFRs when difficult to isolate. b. Magnetic twist at $z = 1, \mathrm{Mm}$. c. Synthetic emissivity from the electric current density. Below panel a are listed values of: W_{tot} and W_{pot}, the magnetic energy of the reconstructed solution and the current-free one for the entire magnetogram; W, the magnetic energy contained in each box; ΔW, the free magnetic energy (compared to the current-free field); W_σ, the semi-open field energy associated with the opening of each box; $|Tw|$, the magnetic twist of the TFR in each box (or the maximum when several are present). All magnetic energies are expressed in erg.

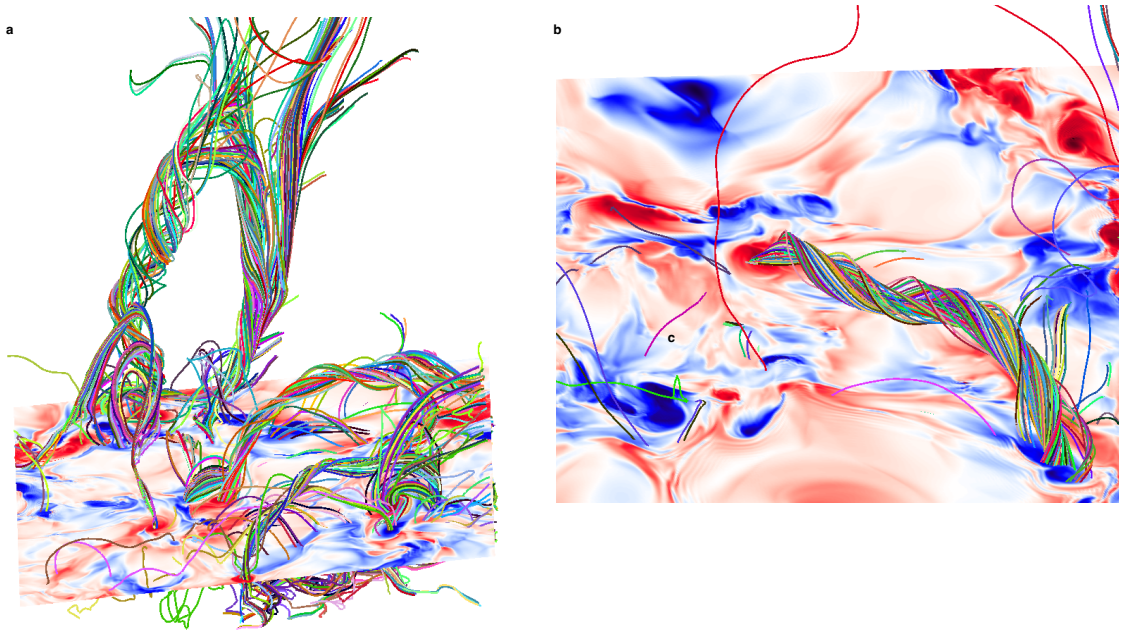

Figure 4. Selected field lines of the magnetic environment above the photosphere during the simulation, taken at two different times and two different view angles. Twisted Flux Ropes (TFRs) around mesospots and below and above the transition regions. The horizontal size of the domain is the same as that of the smallest rectangle drawn in green in Figure 1. For both views a horizontal scalar map of the vertical component of the magnetic field in the high chromosphere.